

Astrophysical Implications of Equation of State for Hadron-Quark Mixed Phase: Compact Stars and Stellar Collapses

Ken'ichiro Nakazato,^{1,*} Kohsuke Sumiyoshi,² and Shoichi Yamada^{1,†}

¹*Department of Physics, Waseda University,
3-4-1 Okubo, Shinjuku, Tokyo 169-8555, Japan*

²*Numazu College of Technology, Ooka 3600, Numazu, Shizuoka 410-8501, Japan*

(Dated: October 30, 2018)

We construct an equation of state including the hadron-quark phase transition. The mixed phase is obtained by the Gibbs conditions for finite temperature. We adopt the equation of state based on the relativistic mean field theory for the hadronic phase taking into account pions. As for the quark phase, the MIT bag model of the deconfined 3-flavor strange quark matter is used. As a result, our equation of state is thermodynamically stable and exhibits qualitatively the desired properties of hadron-quark mixed matter, such as the temperature dependence of the transition density. The pions raise the transition density because they make the equation of state softer. Using the equation of state constructed here, we study its astrophysical implications. The maximum mass of compact stars is investigated, and our equation of state is consistent with recent observations. We also compute the collapse of a massive star with 100 solar masses (M_{\odot}) using our equation of state and find that the interval time from the bounce to the black hole formation becomes shorter for the model with pions and quarks. The pions and quarks affect the total energy of the emitted neutrinos because the duration time of the neutrino emission becomes shorter. The neutrino luminosity rises under the effect of pions since the density of the proto-neutron star becomes high.

I. INTRODUCTION

It has been theoretically suggested that hadronic matter undergoes a deconfinement transition to quark matter at high temperature and/or high density. It is also inferred that the transition occurs inside compact stars [1, 2, 3]. Stars with a quark matter central region and a hadronic matter mantle are called hybrid stars. While the equation of state (EOS) for the hadron-quark mixed phase is not yet fully understood, structures and maximum masses of the hybrid stars have been well studied [4, 5, 6, 7, 8, 9, 10, 11], for review Ref. 12. For the phase transition of a single substance, like a liquid-vapor transition of H_2O , it is simple to treat the mixed phase. On the other hand, in the hadron-quark transition, the substance is composed not only of u quarks but also of d quarks [4]. Incidentally, some authors use the simple Maxwell construction for the studies of hybrid stars [7, 9]. In this scheme, Gibbs conditions for two components are not satisfied completely and EOS's of two phases are connected from the plot of pressure versus chemical potential.

This transition may play an important role in the gravitational collapse of a star, such as a core collapse supernova. In addition, there is a possibility of forming a black hole by the transition because the compact stars have maximum masses. In this case, the EOS with finite temperature and including neutrinos is needed whereas the EOS can be calculated under zero temperature and neutrino-less β equilibrium for hybrid stars. The inclusion of neutrinos is needed because they will be trapped at a very high density as the hadron-quark transition occurs. Moreover, for the gravitational collapse of a star, the EOS should be constructed in a consistent method in the wide range of density. Recently, dynamical simulations of the stellar core collapse including the transition have been done; however, their EOS is obtained at zero temperature and they adopt the Maxwell construction for mixed phase [13, 14]. So far, the stellar collapse including the hadron-quark phase transition with a finite temperature EOS and neutrinos has not been studied.

A study on the mixed phase and hot hybrid stars using Gibbs conditions for finite temperature with neutrinos exists; however, it does not compute the dynamics of the stellar collapse and its EOS does not include low density regime where heavy nuclei appear [5]. In Ref. 5, the relativistic mean field model of the Walecka type is adopted for the EOS of hadronic matter. This model does not take into account the non-linear self-coupling terms of σ meson and ω meson, which are essential to reproduce the properties of nuclei quantitatively and of dense matter in a reasonable manner [15]. In addition, pions are not included in its hadronic phase while they may affect the transition density.

*Electronic address: nakazato@heap.phys.waseda.ac.jp

†Also at Advanced Research Institute for Science & Engineering, Waseda University, 3-4-1 Okubo, Shinjuku, Tokyo 169-8555, Japan.

The color dielectric model is used to describe quark matter. We will revisit this model in Sec. III A comparing with our model.

In this study, we construct the EOS of hadron-quark mixed matter including neutrinos for finite temperature and perform the computations of the stellar collapse and black hole formation. An EOS by Shen et al. (Shen EOS) [16, 17] and the MIT bag model [18] are adopted for nuclear matter and quark matter, respectively. Shen EOS is based on the relativistic mean field theory which includes the non-linear self-coupling terms and takes into account non-uniform matter. It is noted that the table of EOS covers a wide density and temperature range and has been often used in astrophysical simulations. Contributions of thermal pions are added to the original Shen EOS in the current study to examine its effect in the minimum model which assumes that an effective mass of pions is equal to their rest mass in vacuum. Incidentally, hyperons are not included in our hadronic EOS, however, we are planning to investigate their effects in future work [20]. The MIT bag model is characterized by a parameter B , which is called the bag constant and related to the degree of interaction. We calculate the EOS for several values for B and investigate its dependence. We show that our EOS is thermodynamically stable because Gibbs conditions for each particle species are completely satisfied for the mixed phase. After examining the neutron star properties, we apply our EOS to the numerical simulation of the stellar core collapse. It is noted that neutrinos are treated consistently in our simulation. Thus we can evaluate the total energy of the neutrinos emitted from the collapse. We show that the hadron-quark transition affects the dynamics and neutrino emission of the collapse.

In this paper, we perform the computations only for one progenitor model and limited cases of EOS's are used for the hadronic phase and quark phase. This paper is the first stage of the project and we are preparing to study the progenitor dependence [19] and EOS dependence [20] of the collapse and neutrino emission. The final goal of our study is to investigate the effects of the phase transition on the stellar collapse and the possibilities to probe the EOS of hot dense matter from the emitted neutrinos, as demonstrated for pure hadronic matter in Refs. 21, 22.

The organization of this paper is as follows. We devote Sec. II to the formulation of the EOS for the hadron-quark mixed phase. We also introduce EOS's of the pure hadronic and quark matter and present treatments of muons. In Sec. III, we assess our EOS and discuss the dependence on the bag constant, B . As astrophysical implications, we evaluate the maximum mass of the compact stars and investigate the effects of hadron-quark phase transition on the stellar core collapse. Finally, a summary is given in Sec. IV.

II. FORMULATIONS

In this section, we construct the EOS for hadron, quark and their mixture as a function of baryon mass density ρ_B , electron fraction Y_e and temperature T . The EOS calculated in this study covers $10^{5.1} \text{ g cm}^{-3} \leq \rho_B \leq 10^{17} \text{ g cm}^{-3}$, $0 \leq Y_e \leq 0.56$ and $0 \text{ MeV} \leq T \leq 400 \text{ MeV}$. The lower limit of ρ_B and the range of Y_e are the same as those of the Shen EOS, which is adopted for the pure hadronic matter in our model. We assume that the pure hadronic matter exists under the transition density and the pure quark matter exists for a higher density than that of the end point of the mixed phase. In the following, after we introduce the EOS for pure hadronic matter and pure quark matter, we give the formulations of the EOS for mixed matter. Finally, we also describe the treatment of muons.

A. EOS for pure hadronic matter

We adopt the Shen EOS [16, 17] for the pure hadronic matter. This EOS is based on the relativistic mean field theory and the table of EOS covers a wide baryon-mass density range, $\rho_B = 10^{5.1} - 10^{15.4} \text{ g cm}^{-3}$, and temperature range, $T = 0 - 100 \text{ MeV}$. An inhomogeneity of the matter is also taken into account using the Thomas-Fermi approximation because heavy nuclei appear in $T \lesssim 15 \text{ MeV}$ and densities below the nuclear matter density. It is noted that the density where the hadron-quark transition occurs is higher than the nuclear matter density for $T \lesssim 15 \text{ MeV}$ in our model. Thus the hadronic matter at the transition point is composed of dissociated protons and neutrons. It is also noted that we extend the EOS to $T > 100 \text{ MeV}$ by a method fully consistent with the Shen EOS performing the calculations based on the relativistic mean field theory. In this temperature regime, we can regard that the nuclear matter is uniform and the scheme for computations is given in Refs. 23, 24 in detail. The high temperature regime will be revisited in Sec. III A.

We add the effects of charged pions, π^\pm , and neutral pions, π^0 , to the EOS for the pure hadronic matter. The original Shen EOS is based on the mean field theory without the pions. It is noted that the pion field vanishes in the mean field approximation because it is a pseudoscalar particle [25]. In the realistic dense matter, pions may exist though large uncertainties still exist. Thus we examine their qualitative effects by treating them in the minimum model. Here we employ the method in Refs. 25, 26, 27 under the assumption that an effective mass of pions is equal to their rest mass in vacuum. Strictly speaking, pions feel an repulsive potential in the nucleons and their effective mass

gets larger than that in vacuum. In this case, the pion population is suppressed. Thus our assumption corresponds to one extreme case and the situation without pions does the other extreme case [25, 26]. The realistic condition should be between these two cases.

The pions are handled as an ideal boson gas and the chemical potentials of the neutral and charged pions are determined as follows. The chemical potential of the neutral pion is always $\mu_{\pi^0} = 0$ because it is a self-conjugate particle and created by the pair process of two photons. As for the chemical potentials of the charged pions, we set them as $\mu_{\pi^-} = \mu_n - \mu_p$ and $\mu_{\pi^+} = -\mu_{\pi^-}$, where μ_p and μ_n are the chemical potentials of proton and neutron, respectively. When the charge chemical potential, $\mu_n - \mu_p$, exceeds the rest mass of charged pions, m_{π^\pm} , at high densities, the charged pions are condensed and the charge chemical potential decreases to their rest mass. In fact, there is such a regime in the original Shen EOS table. It is well known that this threshold is sensitive to the density dependence of the symmetry energy. We remark that the density dependence is strong in the relativistic nuclear many body frameworks such as the relativistic mean field theory for Shen EOS, as compared with the non-relativistic counter part [28].

In the following, we replace the original Shen EOS given as a function of baryon mass density ρ_B , proton fraction Y_p and temperature T with our hadronic EOS given as a function of ρ_B , Y_C and T . Y_C is a charge fraction and defined as

$$Y_C = \frac{n_p - n_{\pi^-}}{n_B}, \quad (1)$$

where n_B and n_p are the baryon number density and the number density of protons, respectively. n_{π^-} is a net number density of the charged pions, which is the difference of the number density of π^- to that of π^+ , and calculated from the Bose-Einstein distribution function:

$$n_{\pi^-} = \frac{1}{h^3} \int_0^\infty \left[\frac{1}{\left\{ \exp \left(\sqrt{m_{\pi^\pm}^2 c^4 + p^2 c^2} - \mu_{\pi^-} \right) / (k_B T) \right\} - 1} - \frac{1}{\left\{ \exp \left(\sqrt{m_{\pi^\pm}^2 c^4 + p^2 c^2} + \mu_{\pi^-} \right) / (k_B T) \right\} - 1} \right] 4\pi p^2 dp, \quad (2)$$

where h , k_B and c are the Planck constant, the Boltzmann constant and the velocity of light, respectively. When the pions are not condensed, we find μ_{π^-} and the corresponding state of the nucleons in the Shen EOS for given ρ_B , Y_C and T . In this process, we determine the relations of n_p , μ_p and μ_n from the Shen EOS. Using μ_{π^-} found above, the pressure and energy density of the pions are calculated.

On the other hand, in case of the pion condensation, we fix the chemical potential as $\mu_{\pi^-} = m_{\pi^\pm} c^2$ and calculate the number density of the ‘‘thermal’’ pions, $n_{\pi^-}^{\text{th}}$, in Eq. (2). The pressure and energy density of ‘‘thermal’’ pions are given from the Bose-Einstein distribution function as in the case without the pion condensation. At the same time, we can determine the EOS of nucleons for given ρ_B and T using the Shen EOS under the condition of $\mu_n - \mu_p = m_{\pi^\pm} c^2 (= \mu_{\pi^-})$. Having Y_p and n_p fixed, we can get the net number density of the pions, n_{π^-} , for given Y_C using Eq. (1). Here we set the number density of the ‘‘condensed’’ pions as $n_{\pi^-}^{\text{cond}} = n_{\pi^-} - n_{\pi^-}^{\text{th}}$. These condensed pions contribute not to the pressure but to the energy density by their rest masses. We can determine the EOS including condensed pions approximately.

Incidentally, when the electron-type neutrinos are trapped and in equilibrium with other particles, their chemical potential should be given as Eq. (8a), which is expressed later. For high density regime where the hadron-quark transition occurs, neutrinos are fully trapped and we show the results including trapped neutrinos in Sec. III A. On the other hand, since neutrinos are not trapped at least for the onset of gravitational collapse, we follow the time evolution of neutrino distributions through neutrino reactions for numerical simulations in Sec. III C. In addition to the quark degree of freedom, hyperons and kaons also may be important in the high density regime. In particular, since hyperons will appear before the hadron-quark phase transition [27, 29], we are investigating their effects in future work [20].

B. EOS for pure quark matter

We adopt the MIT bag model [18] as the pure quark matter. This is a phenomenological model which describes the nature of the confinement and the asymptotic freedom of quarks. In this model, free quarks are confined in the ‘‘bag’’ and this ‘‘bag’’ has a positive potential energy per unit volume [18]. Thus the thermodynamical potential is

expressed as $\Omega_Q = \Omega_0 + BV$,¹ where V and Ω_0 are the volume of the “bag” and the thermodynamical potential of free quarks as ideal fermions, respectively. The bag constant, B , is a parameter characterizing this model, and we investigate its dependence later. From thermodynamical relations, we can calculate the number density n_Q , pressure P_Q and energy density ε_Q for the quark matter with the temperature T as

$$n_Q = \sum_f \frac{g}{h^3} \int_0^\infty \left(F_f^+(p) - F_f^-(p) \right) 4\pi p^2 dp, \quad (3a)$$

$$P_Q = \sum_f \frac{g}{h^3} \int_0^\infty \frac{p^2 c^2}{3\sqrt{m_f^2 c^4 + p^2 c^2}} \left(F_f^+(p) + F_f^-(p) \right) 4\pi p^2 dp - B, \quad (3b)$$

$$\varepsilon_Q = \sum_f \frac{g}{h^3} \int_0^\infty \sqrt{m_f^2 c^4 + p^2 c^2} \left(F_f^+(p) + F_f^-(p) \right) 4\pi p^2 dp + B, \quad (3c)$$

where $F_f^+(p)$ and $F_f^-(p)$ represent the Fermi-Dirac distribution functions for particle and antiparticle, respectively, and they are expressed as

$$F_f^\pm(p) = \frac{1}{\left\{ \exp \left(\sqrt{m_f^2 c^4 + p^2 c^2} \mp \mu_f \right) / (k_B T) \right\} + 1}. \quad (4)$$

The subscript f denotes the flavor of quarks, and we take into account three flavors, namely, u -, d - and s quarks. The statistical weight is $g = 2 \times 3$. m_f and μ_f are the mass and the chemical potential of f quark, respectively, and we adopt $m_u c^2 = 2.5$ MeV, $m_d c^2 = 5$ MeV and $m_s c^2 = 100$ MeV in this study [30].

As mentioned already, the EOS for the pure hadronic matter is given as the function of the baryon mass density ρ_B , the charge fraction Y_C and the temperature T . We can rewrite the EOS of the MIT bag model as the function of these three independent variables. For convenience, we define the “baryon” number density and the “baryon” mass density of the quark matter as

$$n_{B,Q} = \frac{n_Q}{3}, \quad (5a)$$

$$\rho_{B,Q} = m_{\text{unit}} \frac{n_Q}{3}, \quad (5b)$$

where the value of the atomic mass unit $m_{\text{unit}} = 931.49432$ MeV is used as in the Shen EOS. Since the electric charges of u -, d - and s quarks are $\frac{2}{3}$, $-\frac{1}{3}$ and $-\frac{1}{3}$ of that of a proton, respectively, the charge fraction of the quark matter is as follows:

$$Y_{C,Q} = \frac{2n_u - n_d - n_s}{n_u + n_d + n_s} = \frac{2n_u - n_d - n_s}{n_Q}, \quad (6)$$

where n_f is a number density of f quarks. When the β equilibrium is satisfied, μ_d is equal to μ_s , which is expressed later as Eq. (8d). Thus we can determine μ_u , μ_d and μ_s for given $\rho_{B,Q}$, $Y_{C,Q}$ and T , and we can express P_Q and ε_Q as functions of $\rho_{B,Q}$, $Y_{C,Q}$ and T . We can also calculate other variables, such as the entropy density $s_Q = \frac{P_Q + \varepsilon_Q}{T} + \frac{1}{T} \sum_f n_f \mu_f$, the Helmholtz free energy per unit volume $\mathcal{F}_Q = \varepsilon_Q - T s_Q$ and the Gibbs free energy per unit volume $\mathcal{G}_Q = \mathcal{F}_Q + P_Q$. We will use these variables later in this paper.

C. EOS for hadron-quark mixed phase

Following Ref. 4, we first show the conditions of the equilibrium between phases in the heat bath with the temperature T . Here, we deal with hadronic matter, quark matter, electrons, electron type neutrinos and mu-type leptons, whose treatment is stated later in Sec. IID. We assume that the equilibrium is achieved not only by the strong interactions but also by the weak interactions. This is because only u - and d quarks are deconfined from protons and

¹ Some authors use a formula, which includes the lowest-order gluon interaction with the coupling constant α_s [6, 13, 14]. However, the validity is not guaranteed for the densities in which we are interested because the perturbative approach is valid only in the high energy limit. Hence, we do not take into account these effects in this study.

neutrons and s quarks are created by the weak interactions. Moreover, we assume that the neutrinos are completely trapped owing to high density. In other words, the diffusion time scale is much longer than the reaction time scale. Thus the following reactions are in chemical equilibrium:

$$p + e^- \longleftrightarrow n + \nu_e, \quad (7a)$$

$$n \longleftrightarrow u + 2d, \quad (7b)$$

$$p \longleftrightarrow 2u + d, \quad (7c)$$

$$d \longleftrightarrow u + e^- + \bar{\nu}_e, \quad (7d)$$

$$s \longleftrightarrow u + e^- + \bar{\nu}_e, \quad (7e)$$

$$u + d \longleftrightarrow u + s, \quad (7f)$$

and the relations of the chemical potentials are given as

$$\mu_p + \mu_e = \mu_n + \mu_\nu, \quad (8a)$$

$$\mu_n = \mu_u + 2\mu_d, \quad (8b)$$

$$\mu_p = 2\mu_u + \mu_d, \quad (8c)$$

$$\mu_d = \mu_s. \quad (8d)$$

It is noted that electrons reside in both phases and the chemical potential for each phase coincides with each other. This is also true for neutrinos. It goes without saying that two phases are also in mechanical equilibrium. For simplicity, we ignore the surface tension and the screening of the charged particles though they may affect the EOS [31]. Thus we require the condition,

$$P_H = P_Q, \quad (9)$$

where P_H and P_Q are the pressures of hadronic and quark phases, respectively. It is noted that we do not need to take into account the contribution of leptons in Eq. (9), because their chemical potentials and pressures are the same for each phase.

Next, we relate the independent variables in each phase to the average values using a volume fraction of the quark phase, χ . For instance, a pure hadronic phase corresponds to $\chi = 0$ and a pure quark phase to $\chi = 1$. Then the baryon mass density of the mixed phase, ρ_B , is written as

$$\rho_B = (1 - \chi)\rho_{B,H} + \chi\rho_{B,Q}, \quad (10)$$

where $\rho_{B,H}$ is the baryon mass density of the hadronic phase and $\rho_{B,Q}$ is that of the quark phase and given in Eq. (5b). We note that, the charge fractions of both phases, $Y_{C,H}$ and $Y_{C,Q}$, do not necessarily coincide with each other. Since the mixed phase is charge neutral as a whole, we can relate these values with the electron fraction of the mixed phase, Y_e , as

$$Y_e\rho_B = (1 - \chi)Y_{C,H}\rho_{B,H} + \chi Y_{C,Q}\rho_{B,Q}. \quad (11)$$

It is noted that the charge neutrality is not required for each phase independently [4]. This fact gives an essential difference from the phase transition of a single substance like a liquid-vapor transition of H_2O . For instance, the pressure of the hadron-quark mixed phase is not constant in an isothermal process. Now the construction of the EOS for hadron-quark mixed phase is reduced to the determination of the volume fraction, χ , for given ρ_B , Y_e and T . Mathematically, it is equivalent to solving the system of 5 equations (8b, 8c, 9, 10, 11) for 5 variables, namely, χ , $\rho_{B,H}$, $Y_{C,H}$, $\rho_{B,Q}$ and $Y_{C,Q}$. Here ρ_B and Y_e are given, μ_n , μ_p and P_H are the functions of $\rho_{B,H}$ and $Y_{C,H}$, and μ_u , μ_d and P_Q are the functions of $\rho_{B,Q}$ and $Y_{C,Q}$.

D. Treatment of muons

As mentioned already, the treatment of muons and their anti-particles is important because their compositions affect the EOS. In this study, we examine two situations.

The first one corresponds to the EOS for stellar core collapse. Here, we call it supernova (SN) matter. In the case of an ordinary supernova, it is known that not only the net muon fraction but also the muon and anti-muon fractions themselves are minor because the rest mass of the muon is large ($m_\mu = 105.66$ MeV). Then, they are omitted in simulations for the ordinary supernova. On the other hand, we may not be able to neglect their effects for EOS

in case of black hole formation, because the density and temperature would be higher than those for the ordinary supernova [32, 33].

During the core collapse and bounce, muons behave as follows. Since the charged current reactions for mu-type leptons are not efficient before neutrino trapping, mu-type neutrinos (ν_μ) and their anti-particles ($\bar{\nu}_\mu$) are produced mainly by pair processes, and their reactions are almost identical. Thus one can safely posit that the net muon fraction is zero during the initial collapse before neutrino trapping. When neutrinos are fully trapped, the charged current reactions may become efficient. Therefore, muons and mu-type neutrinos are in chemical equilibrium. ν_μ and $\bar{\nu}_\mu$ cannot be regarded as identical, and the net muon fraction can become non-zero.

In this study, in order to add the effects of muon and anti-muon pairs in a tractable manner, we do not assume chemical equilibrium for muon type leptons² but suppose that the net muon fraction is zero (i.e., $\mu_\mu = 0$). The approximation $\mu_\mu = 0$ is reasonable because the pair population dominates in higher temperature regime, where we cannot neglect the effects of muon-type leptons for EOS in the black hole formation. Incidentally, this assumption is consistent with the methods of our simulations stated in Sec. III C, which does not take into account the muon-charged current reactions. In order to treat the muon-charged current reactions, one has to solve the neutrino-transfer for 6 species, which requires formidable computing resources. It is also necessary to prepare the EOS table as a function of not only Y_e but also Y_μ , which makes the setups further complicated. The muon-charged current reactions should be included in future to assess their effects.

The second case of the treatment of muons is for so-called neutron star (NS) matter. In this case, the neutrino less β equilibrium at zero temperature is achieved and the chemical potential of the muons, μ_μ , is the same as that of electrons. Thus the relations of the chemical potentials become as follows:

$$\mu_e = \mu_n - \mu_p, \quad (12a)$$

$$\mu_\mu = \mu_e. \quad (12b)$$

Moreover, the charge neutrality condition (11) is modified to

$$(Y_e + Y_\mu)\rho_B = (1 - \chi)Y_{C,H}\rho_{B,H} + \chi Y_{C,Q}\rho_{B,Q}, \quad (13)$$

where Y_μ is a muon fraction.

III. RESULTS

In this section, we show the features of the EOS described in the preceding section. We choose a mixed EOS with the hadronic matter including pion and the quark matter of the bag constant $B = 250 \text{ MeV fm}^{-3}$ ($B^{1/4} = 209 \text{ MeV}$), as a reference model. This value is adopted in another recent study on the hadron-quark phase transition [34]. Here we discuss the properties of EOS with the applications to the maximum mass of compact stars and a stellar collapse. We mainly show the results of the reference model for the NS matter and the SN matter. Incidentally, results of the model without pions are also shown, and the dependence on the bag constant is studied for several topics. Further studies on stellar collapse will be reported elsewhere [19, 20].

A. Assessments of EOS

First of all, we examine the composition of our EOS for NS matter and SN matter to compare with other EOS's in the previous studies using similar schemes [4, 5, 9, 27]. For SN matter, we show the cases of $T = 50 \text{ MeV}$ with the electron type lepton fraction $Y_l = 0.1$, where Y_l is defined as the sum of the electron fraction, Y_e , and the electron-type neutrino fraction, Y_{ν_e} . Note that when the neutrinos are fully trapped, Y_l is conserved for each fluid element in the stellar core. In FIG. 1, we show the particle fractions, $Y_i \equiv \frac{n_i}{n_B}$, where n_i represents the number density of the particle i , for the reference models. When pions begin to condensate in the NS matter, the proton fraction increases and the fractions of electron and muon decrease [27]. At the onset of the hadron-quark phase transition, d quarks have larger population than those of u - and s quarks not only for the NS matter [4] but also for the SN matter [5]. In the pure quark phase, the number ratio of u -, d - and s quark is nearly equi-partition and the relation, $Y_s < Y_u < Y_d$ holds for

² We remark that the β equilibrium assumed in previous sections is for the electron-type leptons. This assumption is not inconsistent with the treatment of muons.

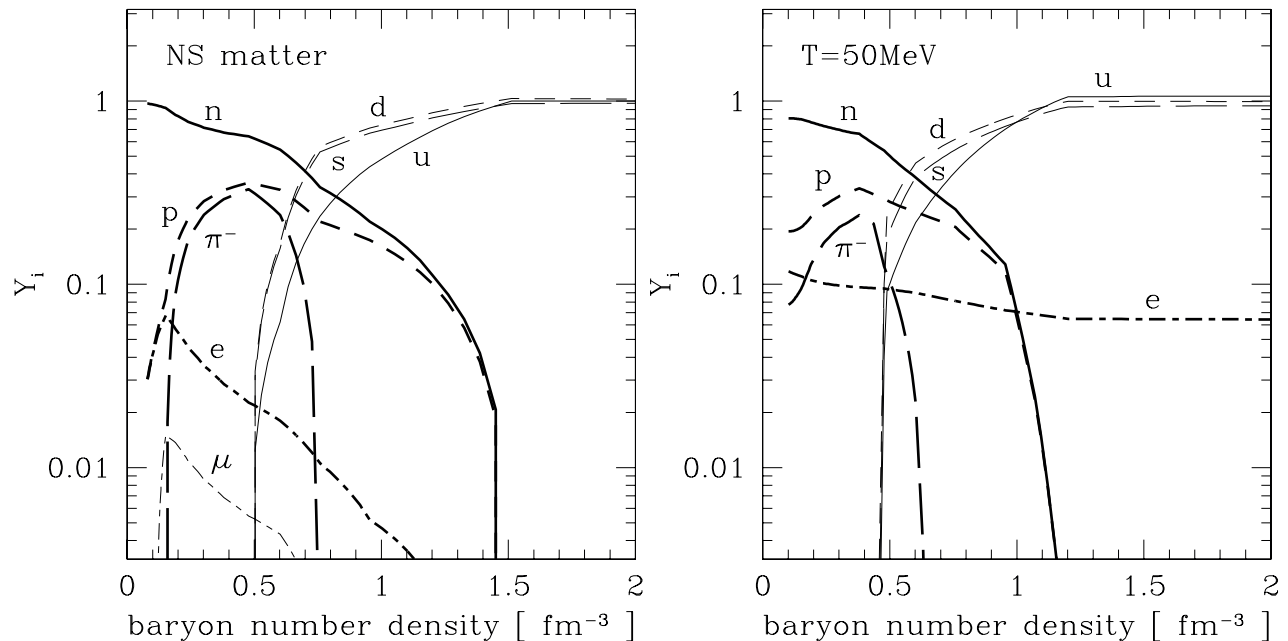


FIG. 1: Particle fractions for the reference model of NS matter (left) and SN matter with $T = 50$ MeV and $Y_l = 0.1$ (right). The particle fraction, Y_i , is defined as $\frac{n_i}{n_B}$, where n_i represents the number density of the particle i .

the NS matter. For the SN matter with neutrino trapping, u quarks have larger population than those of d - and s quarks [5, 9]. All of these features are consistent with the previous results.

In FIG. 2, we compare the EOS for the reference model with those for pure hadronic and quark matters, where the bag constant $B = 250$ MeV fm^{-3} . This figure illustrates both for NS matter and SN matter with $T = 20, 50$ and 120 MeV and $Y_l = 0.1$. As mentioned already, the pressure of the hadron-quark mixed phase is not constant in an isothermal process [4], which is well presented in our models. In addition, this trend is shown also in the other previous work [6] while the bag constant is different from ours. The internal energy, which is the difference of the energy density with respect to $\rho_B c^2$, of the mixed phase is larger than that of the hadronic phase for high temperature regime ($T \geq 50$ MeV). This is not unphysical because we should compare not the internal energies but the free energies. In the left panels of FIG. 3, we show the Helmholtz free energies per baryon as a function of the specific volume. If the EOS is thermodynamically stable, this function is convex downward. This feature is fulfilled for our models. In the right panels of FIG. 3, on the other hand, we show the Gibbs free energies per baryon as a function of the pressure. We can recognize that the free energies of the mixed phase are always lower than those of the pure hadronic and quark phases.

For the phase transition of matter with two components, it is known that the mixed phase should satisfy not only the condition of mechanical stability, as verified above, but also the stability with respect to diffusion [35]. In our model, the condition is expressed as

$$\left(\frac{\partial \mu_n}{\partial X_p} \right)_{P,T} \leq 0, \quad (14)$$

where X_p is a “total” proton fraction and defined as

$$X_p = \frac{1}{n_B} \left(n_p + \frac{2n_u - n_d - n_s}{3} \right). \quad (15)$$

This feature is shown for our results in FIG. 4 and satisfied also in other ranges of the parameters. The reference model of the SN matter with $Y_l = 0.1$ for fixed pressure and temperature are indicated in this figure. From these analyses, we can confirm that our EOS is thermodynamically stable.

In FIG. 5, we show the temperature dependences of the transition density and the critical baryon chemical potential for our EOS of the SN matter with $Y_l = 0.1$ and 0.3 . These phase diagrams are given not only for the reference model but also for a model without pions while the bag constant of both models is 250 MeV fm^{-3} . The baryon chemical

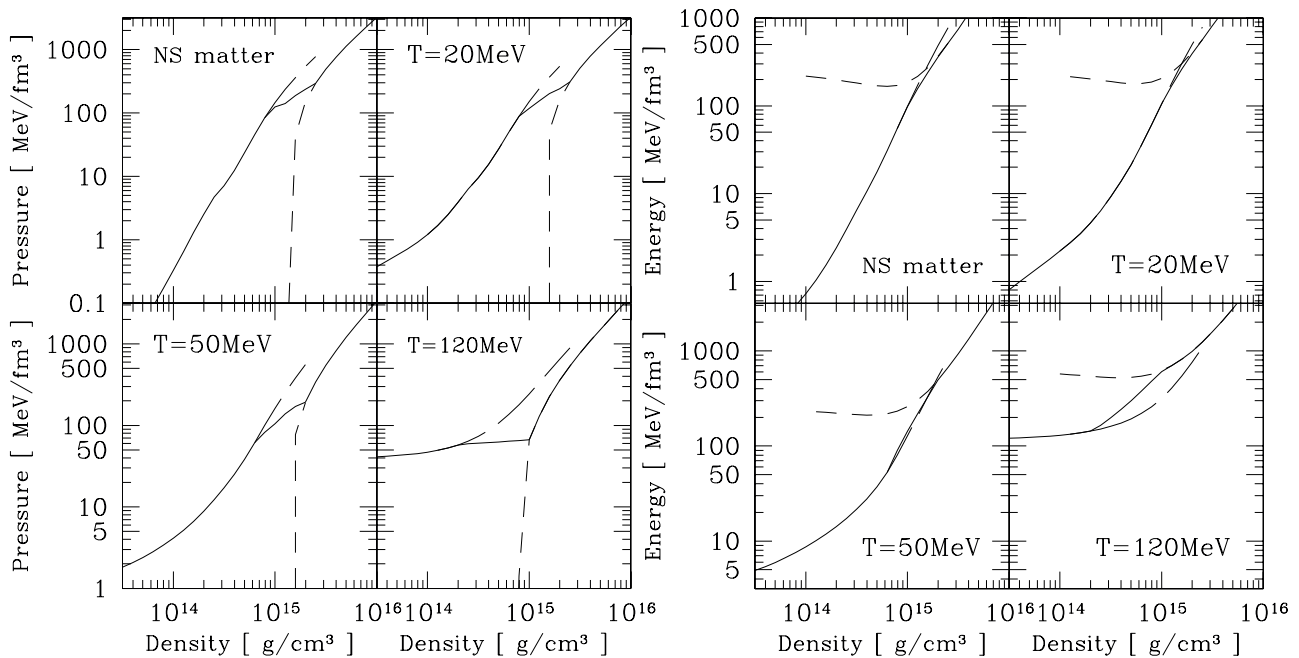


FIG. 2: EOS's for mixed matter (solid lines), pure hadronic matter (long-dashed lines) and pure quark matter (short-dashed lines). In all panels, the bag constant is chosen as $B = 250 \text{ MeV fm}^{-3}$ for the quark model. The left and right panels show the pressure and the internal energy, respectively, as a function of the density. In both panels, the upper left, the upper right, the lower left and the lower right plots correspond to the reference models of NS matter, SN matter with $T = 20, 50$ and 120 MeV , respectively. The electron type lepton fraction, Y_l , is fixed to 0.1 for all models of SN matter.

potential in these figures, μ_B , is the same as the neutron chemical potential in the preceding sections, μ_n . We can see that the reference model has larger transition density and baryon chemical potential than those of the model without pions. This is because pions make the EOS softer; in other words, pressure gets lower for a fixed baryon number density. Thus the condition of equilibrium (9) is satisfied for larger density. Incidentally, the phase diagram has been studied in Ref. 5 while its EOS for hadronic matter does not include pions. The color dielectric model is used for the quark matter model whereas we use the MIT bag model. In Ref. 5, the transition density gets lower at higher temperature, which is the same as our result, however, its transition density is lower than ours, especially at finite temperature. For instance, the transition density is $\sim 10^{14} \text{ g cm}^{-3}$ at $T \sim 30 \text{ MeV}$.

It is suggested that the transition line has an end point in the high temperature regime. The nature of the transition changes at this point, while the exact phase diagram is not well known. This is a so-called critical point. The temperature of the critical point, T_c , is investigated experimentally by heavy-ion collisions [36, 37] and theoretically by lattice QCD calculations [38, 39, 40, 41]. From these studies, it may be in the range, $150 \text{ MeV} \leq T_c \leq 200 \text{ MeV}$. Above the critical temperature, the quark phase may be the most stable state for any densities. It is also suggested that the baryon chemical potential of the critical point is much smaller than the typical hadronic scale, $\mu_B \lesssim 40 \text{ MeV}$. Although our model cannot describe the critical point in detail, the critical baryon chemical potential drops dramatically with the temperature in the regime $T \gtrsim 100 \text{ MeV}$. For much higher temperature regime, the quark matter is more stable than the hadronic matter even at zero density. As shown in FIG. 6, for instance, the hadron-quark phase transition occurs at $T = 150 \text{ MeV}$ and the quark phase is always the most stable state at $T = 200 \text{ MeV}$ for the model with $B = 250 \text{ MeV fm}^{-3}$. Therefore, the plots for $T \gtrsim 150 \text{ MeV}$ are not given in FIG. 5. In this study, the bag constant B is independent of the temperature and the temperature at which the quark matter becomes most stable depends solely on B . The larger the value of B , the higher this temperature becomes. When this temperature is in the range $150 \text{ MeV} \leq T \leq 200 \text{ MeV}$, the bag constant is in $210 \text{ MeV fm}^{-3} \lesssim B \lesssim 650 \text{ MeV fm}^{-3}$ ($200 \text{ MeV} \lesssim B^{1/4} \lesssim 265 \text{ MeV}$) for our models. It is noted that the bag constant of the reference model, $B = 250 \text{ MeV fm}^{-3}$ ($B^{1/4} = 209 \text{ MeV}$), lies within this range.

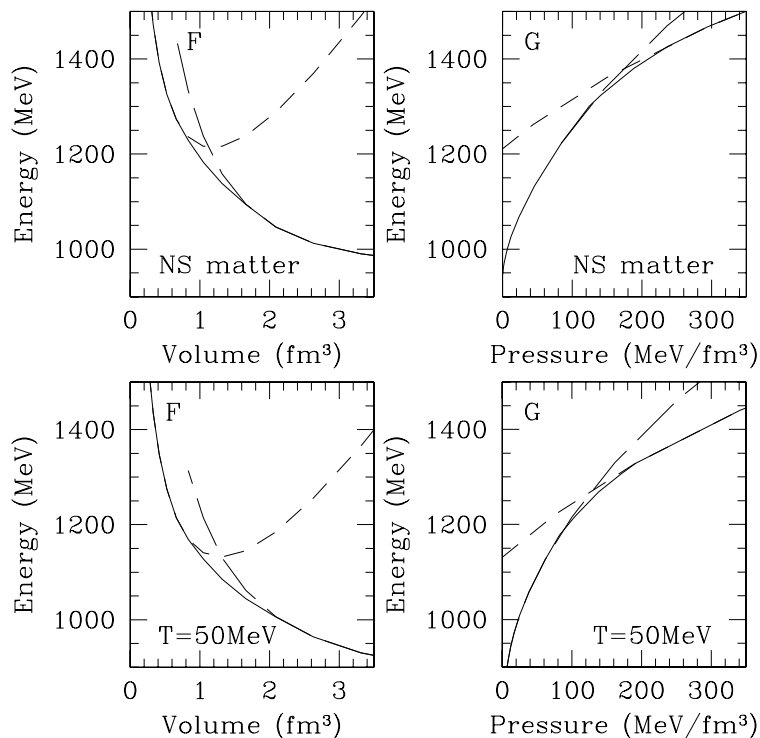


FIG. 3: EOS's for mixed matter (solid lines), pure hadronic matter (long-dashed lines) and pure quark matter (short-dashed lines). In all panels, the bag constant is chosen as $B = 250 \text{ MeV fm}^{-3}$ for the quark model. The upper left and upper right panels show the Helmholtz free energies per baryon (F) as a function of a specific volume of the system and the Gibbs free energies per baryon (G) as a function of the pressure, respectively, for the reference model of NS matter. The lower two panels are the same as upper two panels but for the reference model of SN matter with $T = 50 \text{ MeV}$ and $Y_l = 0.1$.

B. Maximum mass of the hybrid stars

We examine the maximum mass of hybrid stars constructed by our EOS for NS matter. In the following, we denote the EOS's without pions and quarks (the original Shen EOS [16, 17]), without pions but with quarks, with pions and without quarks and the model with pions and quarks (the reference model) as OO, OQ, PO and PQ, respectively. The bag constant is $B = 250 \text{ MeV fm}^{-3}$ for the models with quarks. In FIG. 7, we show the mass-radius trajectories for our EOS's together with the recent data of compact star masses. We can see that the pion population and the hadron-quark transition lower the maximum mass because they soften the EOS. For instance, the maximum mass of model OO is $2.2 M_\odot$ while those of models PO, OQ and PQ are $2.0 M_\odot$, $1.8 M_\odot$ and $1.8 M_\odot$, respectively. In the right panel, we show the dependence on B . We can see that the maximum mass becomes lower when the bag constant becomes small. This is because the phase transition density is lower for smaller bag constants.

The recent measurements of compact star masses increase the lower limit of the maximum mass. For instance, it has been established with 95% confidence that at least one of the two pulsars, Ter 5 I and J, is more massive than $1.68 M_\odot$ from analysis of the joint probabilities [42]. For the neutron star EXO 0748-676, it has been reported that the lower limits on the mass and radius are $M \geq 2.10 \pm 0.28 M_\odot$ and $R \geq 13.8 \pm 1.8 \text{ km}$ with 1σ error bars, while there are uncertainties in the analysis of the X-ray burst spectra [43]. We note that the reference model ($B = 250 \text{ MeV fm}^{-3}$) is consistent with these measurements whereas models with lower bag constants $B \lesssim 200 \text{ MeV fm}^{-3}$ in our study produce lower maximum masses.

C. Application to stellar core collapse

Recently, numerical studies on black hole formation by stellar core collapse have been done for massive stars with an initial mass of $\sim 40 M_\odot$ [21, 22, 44, 45]. The realistic EOS and the realistic progenitor models are used in the studies of spherically symmetric collapse in Refs. 21, 22 whereas the parametric EOS and polytropic initial model

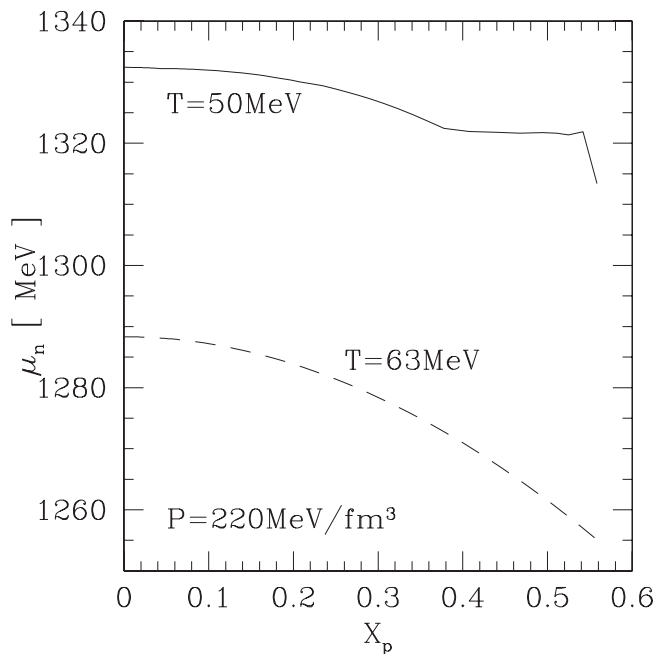


FIG. 4: Profiles of neutron chemical potential, μ_n , as a function of “total” proton fraction, X_p , for fixed pressure $P = 220 \text{ MeV fm}^{-3}$ and temperatures $T = 50 \text{ MeV}$ (solid line) and 63 MeV (dashed line). This is a result for the reference model of SN matter with $Y_l = 0.1$.

are employed in those of axisymmetric collapse in Refs. 44, 45. Collapse of very massive $\sim 300M_\odot$ first generation stars in the universe (so-called Population III stars) have been also studied [46, 47, 48, 49]. It is noted that these studies do not include the hadron-quark phase transition. In this study, we perform numerical simulations for a spherically symmetric stellar collapse using the EOS’s examined in the preceding section. We set the bag constant $B = 250 \text{ MeV fm}^{-3}$ for all the models with quarks. A result of an evolutionary calculation for a Population III star with $M = 100M_\odot$ [50] is chosen as the initial model of our simulation. This model is the intermediate one between the models stated above. The numerical simulation of its collapse has been already done under the Shen EOS [33].

We follow the scheme of Ref. 33 in our simulations. We solve the general relativistic hydrodynamics and neutrino transfer equations simultaneously under spherical symmetry [51, 52]. Neutrino reactions are treated in detail [32]. Incidentally, we have assumed for the EOS that the electron-type neutrinos are in equilibrium with other particles in the hadron-quark mixed phase and the pure quark phase. Hence after the phase transition occurs, we do not compute the neutrino distribution functions and assume that they are Fermi-Dirac functions for all species conserving the electron-type lepton fraction, Y_l , for each fluid element. Moreover, we neglect the entropy variation from the neutrino transport. We can justify this gap in the neutrino treatments because the density is high enough for neutrinos to be trapped anyway at the phase transition. It is also noted that we can compute the collapse up to the apparent horizon formation, which is a sufficient condition for the formation of a black hole. For the details of our simulation such as the initial condition, numerical methods and convergences, see Ref. 33.

In FIG. 8, we show the time profiles of the central baryon mass density. These models have a bounce owing to thermal nucleons at subnuclear density ($\sim 1.4 \times 10^{14} \text{ g cm}^{-3}$) and then recollapse to a black hole. The contribution of pions makes a difference at $\sim 2 \times 10^{14} \text{ g cm}^{-3}$ and that of quarks does so for larger density. We can also see that the effect of quarks begins to work suddenly at the transition density whereas that of pions does gradually. This is because the thermal pions appear before the pion condensation. We note that the duration of neutrino emission is almost the same as the interval time from the bounce to the apparent horizon formation [21, 22]. In Table I, we show them for all models computed here. Since the EOS becomes softer owing to the contribution of pions and quarks, the interval time becomes shorter. Model OO (the original Shen EOS) takes 20% longer to recollapse than model PQ (the reference model in this study) does. Using this difference of the interval time, we may be able to probe observationally the EOS of hot dense matter in future.

The total neutrino energies emitted from each model are shown in Table I. In this simulation, we assume that ν_τ ($\bar{\nu}_\tau$) is the same as ν_μ ($\bar{\nu}_\mu$), and the luminosities of ν_μ and $\bar{\nu}_\mu$ are almost identical. This is because they have the same kind of reactions and the difference of coupling constants is minor. Therefore we denote these four species as

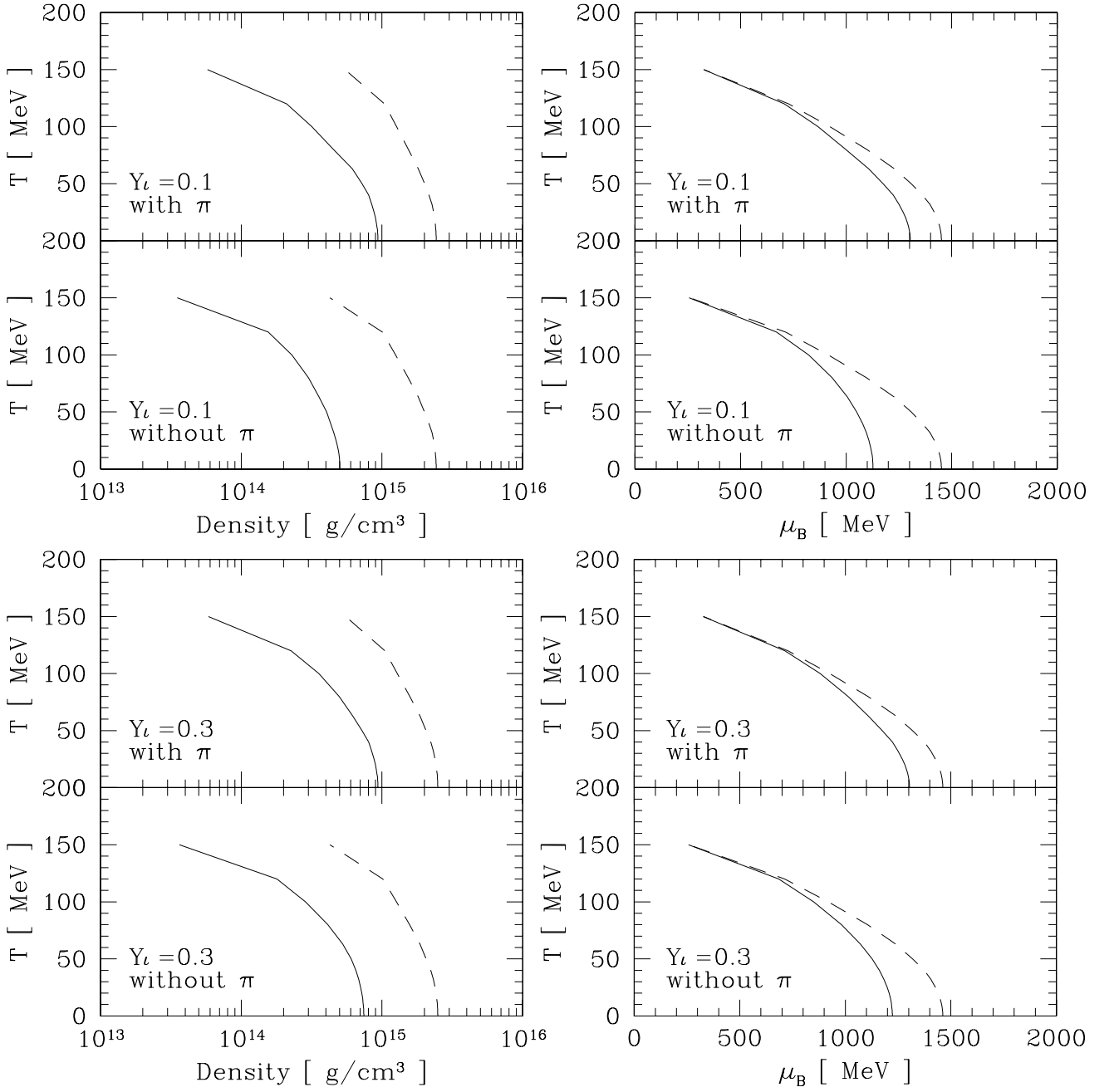


FIG. 5: Phase diagrams of our EOS of the SN matter with $Y_l = 0.1$ and 0.3 for $T < 150$ MeV. Solid lines represent boundaries of hadronic matter and mixed matter and dashed lines do those of mixed matter and quark matter. For the upper plots in each panel, an EOS with pions is used while an EOS without pions is used for the lower plots in each panel. $B = 250 \text{ MeV fm}^{-3}$ is chosen for the bag constant for all panels.

ν_x collectively in Table I, taking the average. Comparing models OO and OQ or models PO and PQ in Table I, we can see that the total energies of emitted neutrinos for the models including quarks become lower than those of the models without quarks. This is because the collapse is hastened by quarks, and their effects make differences only for the last moment as discussed above. Thus the duration of the neutrino emission becomes shorter while the neutrino luminosity does not change much.

This trend can be seen in the effects of pions also. However, the neutrino luminosity for the models with pions differs gradually in time from that for the models without pions because the effect of pions works gradually. The neutrino luminosity summed over all species is given approximately by the accretion luminosity $L_\nu^{\text{acc}} \sim GM_\nu \dot{M}/R_\nu$

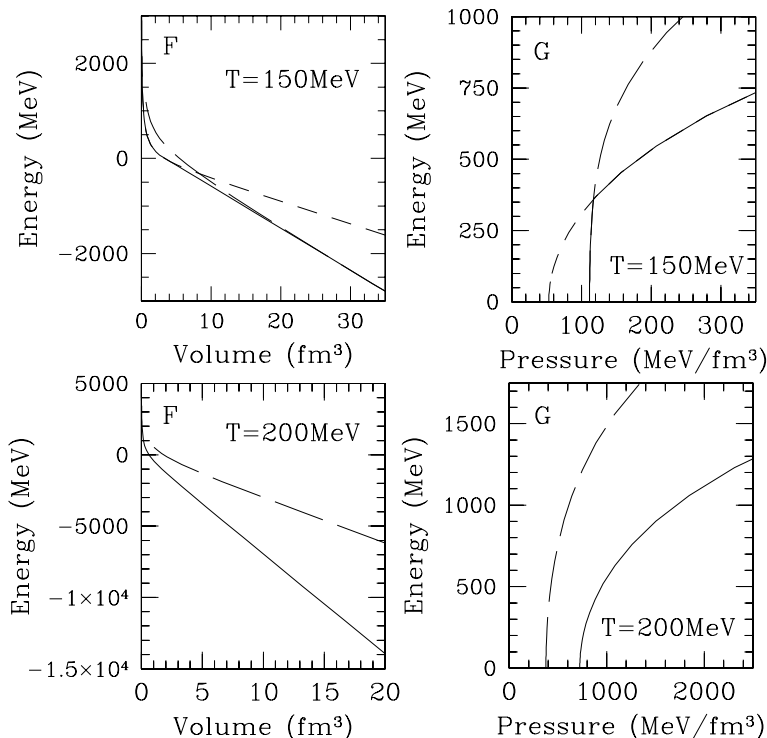


FIG. 6: Same as FIG. 3 but for SN matter with $T = 150$ MeV and $Y_l = 0.1$ (upper panels), and for SN matter with $T = 200$ MeV and $Y_l = 0.1$ (lower panels).

TABLE I: Results of the numerical simulations. The definition of the models is given in the text (Sec. III B). t_{rec} represents the interval time from the bounce to the apparent horizon formation. E_{ν_i} is the total energy of emitted ν_i , where $E_{\nu_x} = E_{\nu_\mu} = E_{\bar{\nu}_\mu} = E_{\nu_\tau} = E_{\bar{\nu}_\tau}$. E_{all} is the total energy summed over all species.

Model	t_{rec} (msec)	E_{ν_e} (ergs)	$E_{\bar{\nu}_e}$ (ergs)	E_{ν_x} (ergs)	E_{all} (ergs)
OO	402	9.42×10^{52}	7.89×10^{52}	4.40×10^{52}	34.9×10^{52}
OQ	352	8.03×10^{52}	6.58×10^{52}	3.44×10^{52}	28.4×10^{52}
PO	351	8.05×10^{52}	6.63×10^{52}	3.67×10^{52}	29.3×10^{52}
PQ	336	7.60×10^{52}	6.22×10^{52}	3.34×10^{52}	27.2×10^{52}

[53], where G , R_ν , \dot{M} and M_ν are the gravitational constant, the radius of the neutrino sphere, the mass accretion rate and the mass enclosed by R_ν , respectively. We can roughly regard the neutrino sphere as the surface on which neutrinos are emitted, and R_ν is defined as,

$$\int_{R_\nu}^{R_s} \frac{dr}{l_{\text{mfp}}(r)} = \frac{2}{3}, \quad (16)$$

where R_s is the stellar radius and l_{mfp} is the mean free path of neutrino. Incidentally in our case, as is the case for an ordinary supernova, the proto-neutron star is formed before the black hole formation, and neutrinos are emitted mainly on the surface of the proto-neutron star. Thus we can regard R_ν and M_ν as the radius and mass of the proto-neutron star, respectively. On the other hand, the density of the proto-neutron star of the model with pions is greater than that of the model without pions comparing at the same time because the EOS becomes soft under the influence of pions as seen in FIG. 8. Thus the radius of the proto-neutron star becomes smaller without changing the mass of it. As a result, the neutrino luminosity gets higher for the models including pions. For instance, at 300 ms after the bounce, the luminosity of model OO is 1.09×10^{53} erg s $^{-1}$ whereas that of model PO is 1.27×10^{53} erg s $^{-1}$. While a simple comparison cannot be done because the quarks also affect the neutrino emission slightly, we can see that model PO has higher total energy than that of model OQ although the interval times are almost the same. In

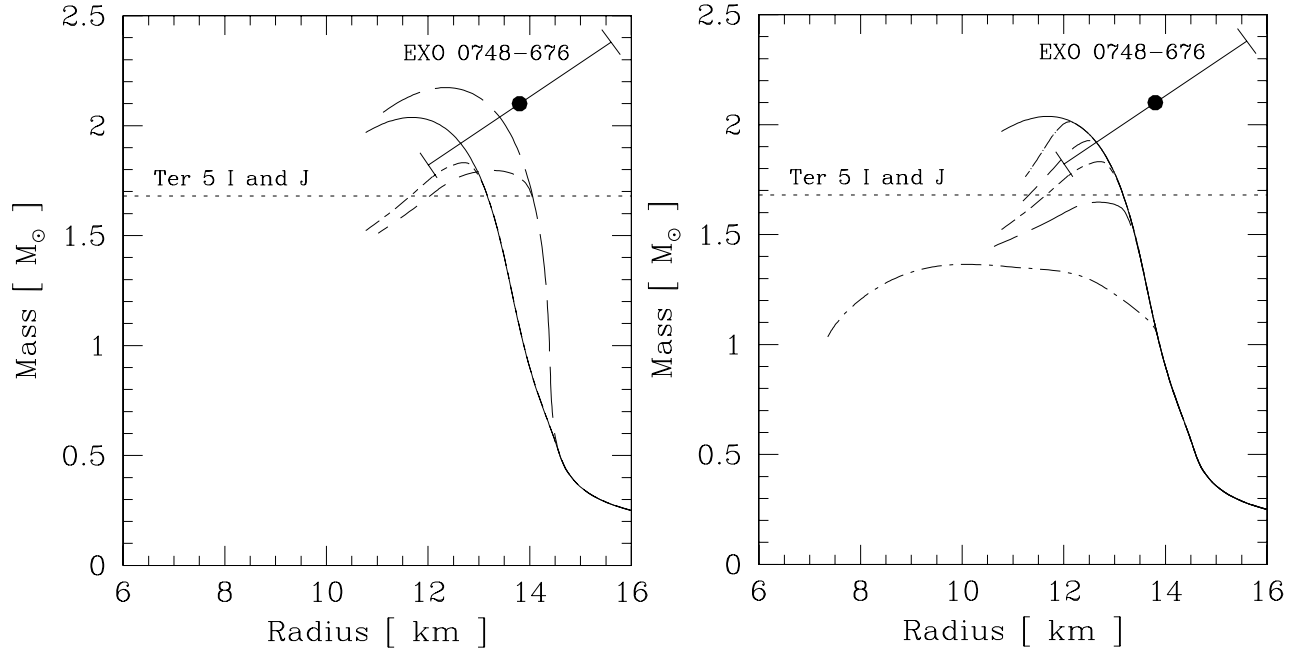


FIG. 7: Mass-radius trajectories for our EOS's of NS matter. In the left panel, long-dashed, short-dashed, solid and dot-dashed lines represent the models OO (the original Shen EOS [16, 17]), OQ, PO and PQ (the reference model), respectively, where the definition of the models is given in the text. In the right panel, we show the results of the models with pions, and the solid line is the same as that in the left panel (PO). Other lines correspond, from bottom to top, to the models with pions and quarks with $B = 150, 200, 250, 300, 400 \text{ MeV fm}^{-3}$. In both panels, horizontal dotted lines represent the lower limit of the maximum mass of compact stars determined by pulsars Ter 5 I and J with 95% confidence, and the plots with 1σ error bars are for the measurements of neutron star EXO 0748-676.

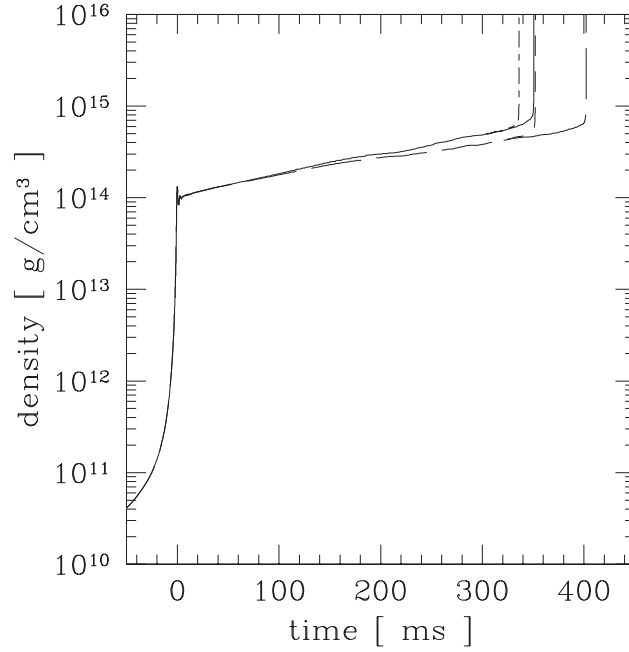


FIG. 8: Time profiles of the central baryon mass density. The notation of the lines is the same as in the left panel of FIG. 7 and the time is measured from the point at bounce.

conclusion, pions make the total energy of the emitted neutrinos lower by shortening the interval time and higher by increasing luminosity.

The computations shown here are done for only a single model, $M = 100M_{\odot}$ and the bag constant $B = 250 \text{ MeV fm}^{-3}$. For the models with a smaller bag constant, an interval time of the neutrino emission may become much shorter because of the smaller maximum mass of the hybrid stars. It is noted that we are preparing more detailed studies for various cases of stellar collapse [19, 20].

IV. SUMMARY

We have constructed the EOS including the hadron-quark phase transition using Gibbs conditions for finite temperature. As for the hadronic phase, we have added pions to the EOS by Shen et al. [16, 17], which is based on the relativistic mean field theory. Our results are found to reproduce the composition in the previous studies particularly for the pion population in the neutrino-less β equilibrium state at zero temperature [27]. As for the quark phase, we have adopted the MIT bag model of the deconfined 3-flavor strange quark matter [18] and the bag constant has set to be $B = 250 \text{ MeV fm}^{-3}$ for the reference model. As for the mixed phase, we have assumed that the equilibrium is achieved not only by the strong interactions but also by the weak interactions. Electrons and electron-type neutrinos are taken into account as being in weak equilibrium for the mixed phase and pure quark phase. Incidentally, we have treated the muons approximately. Our EOS is thermodynamically stable and exhibits qualitatively the desired properties of hadron-quark mixed matter, such as the temperature dependence of the transition density.

We have studied the astrophysical implications of the calculated EOS. The most important effect of pions and quarks is to soften the EOS. Pions and quarks make the maximum mass of compact stars smaller. It is noted that the models including pions and quarks with the bag constant $B \lesssim 200 \text{ MeV fm}^{-3}$ give the maximum mass that is smaller than the recent measurements of compact stars. We have computed the collapse of a massive star with $100M_{\odot}$ using our EOS and found that the interval time from the bounce to the black hole (apparent horizon) formation becomes shorter by the inclusion of pions and quarks. As a result, they affect the total energy of the emitted neutrinos because of the shorter duration. We have also shown that the neutrino luminosity becomes higher under the effect of pions because they raise the density of the proto-neutron star core. We stress that we may be able to discuss the EOS of hot dense matter detecting the neutrinos from black hole progenitors in future.

The current paper is the first attempt to clarify the effects due to the quark-hadron phase transition on the black hole formation and the neutrino emission. We are planning to study the initial mass dependence [19] and the bag constant dependence [20] of stellar core collapse systematically. We will also investigate effects of hyperons in the hadronic matter [20]. There are more problems to be solved regardless of our project. For instance, other quark models like a color superconducting phase and effects of surface tension and screening of charged particles on the equilibrium condition in the mixed phase are worth investigating.

Acknowledgments

We are grateful to Hideyuki Umeda for providing a progenitor model. We would like to thank Akira Ohnishi, Yoshiaki Koma and Chikako Ishizuka for fruitful discussions. Numerical computations were performed on the Fujitsu VPP5000 at the Center for Computational Astrophysics (CfCA) of the National Astronomical Observatory of Japan (VPP5000 System projects ikn18b, ukn08b, iks13a, uks06a), and partially on the supercomputers in JAERI, YITP and KEK (KEK Supercomputer project 108). This work was partially supported by Japan Society for Promotion of Science (JSPS) Research Fellowship, Grants-in-Aid for the Scientific Research from the Ministry of Education, Science and Culture of Japan (14740166, 15540243, 15740160, 17540267, 18540291, 18540295, 19540252) and the 21st-Century COE Program ‘‘Holistic Research and Education Center for Physics of Self-organization Systems.’’

-
- [1] N. Itoh, Prog. Theor. Phys. **44**, 291 (1970).
 - [2] E. Witten, Phys. Rev. D **30**, 272 (1984).
 - [3] F. Weber, Prog. Part. Nucl. Phys. **54**, 193 (2005).
 - [4] N. K. Glendenning, Phys. Rev. D **46**, 1274 (1992).
 - [5] A. Drago and U. Tambini, J. Phys. G **25**, 971 (1999).
 - [6] G. F. Burgio, M. Baldo, P. K. Sahu, and H.-J. Schulze, Phys. Rev. C **66**, 025802 (2002).
 - [7] C. Marieron, M. Baldo, G. F. Burgio, and H.-J. Schulze, Phys. Rev. D **70**, 043010 (2004).
 - [8] D. Blaschke, S. Fredriksson, H. Grigorian, A. M. Öztas, and F. Sandin, Phys. Rev. D **72**, 065020 (2005).

- [9] O. E. Nicotra, M. Baldo, G. F. Burgio, and H.-J. Schulze, *Phys. Rev. D* **74**, 123001 (2006).
- [10] M. Baldo, G. F. Burgio, P. Castorina, S. Plumari, and D. Zappalá, *Phys. Rev. C* **75**, 035804 (2007).
- [11] F. Sandin and D. Blaschke, *Phys. Rev. D* **75**, 125014 (2007).
- [12] N. K. Glendenning, *Compact Stars: Nuclear Physics, Particle Physics and General Relativity* (New York: Springer, 2002).
- [13] N. A. Gentile, M. B. Aufderheide, G. J. Mathews, F. D. Swesty, and G. M. Fuller, *Astrophys. J.* **414**, 701 (1993).
- [14] N. Yasutake, K. Kotake, M. Hashimoto, and S. Yamada, *Phys. Rev. D* **75**, 084012 (2007).
- [15] Y. Sugahara and H. Toki, *Nucl. Phys. A* **579**, 557 (1994).
- [16] H. Shen, H. Toki, K. Oyamatsu, and K. Sumiyoshi, *Nucl. Phys. A* **637**, 435 (1998a).
- [17] H. Shen, H. Toki, K. Oyamatsu, and K. Sumiyoshi, *Prog. Theor. Phys.* **100**, 1013 (1998b).
- [18] A. Chodos, R. L. Jaffe, K. Johnson, C. B. Thorn, and V. F. Weisskopf, *Phys. Rev. D* **9**, 3471 (1974).
- [19] K. Nakazato, K. Sumiyoshi, and S. Yamada (2008a), in prep.
- [20] K. Nakazato, K. Sumiyoshi, and S. Yamada (2008b), in prep.
- [21] K. Sumiyoshi, S. Yamada, H. Suzuki, and S. Chiba, *Phys. Rev. Lett.* **97**, 091101 (2006).
- [22] K. Sumiyoshi, S. Yamada, and H. Suzuki, *Astrophys. J.* **667**, 382 (2007).
- [23] K. Sumiyoshi and H. Toki, *Astrophys. J.* **422**, 700 (1994).
- [24] K. Sumiyoshi, H. Kuwabara, and H. Toki, *Nucl. Phys. A* **581**, 725 (1995a).
- [25] N. K. Glendenning, B. Banerjee, and M. Gyulassy, *Ann. Phys.* **149**, 1 (1983a).
- [26] N. K. Glendenning, P. Hecking, and V. Ruck, *Ann. Phys.* **149**, 22 (1983b).
- [27] N. K. Glendenning, *Astrophys. J.* **293**, 470 (1985).
- [28] K. Sumiyoshi, K. Oyamatsu, and H. Toki, *Nucl. Phys. A* **595**, 327 (1995b).
- [29] S. Balberg, I. Lichtenstadt, and G. B. Cook, *Astrophys. J. Suppl.* **122**, 515 (1999).
- [30] W.-M. Yao, *et al.*, (Particle Data Group), *J. Phys. G* **33**, 1 (2006).
- [31] T. Endo, T. Maruyama, S. Chiba, and T. Tatsumi, *Prog. Theor. Phys.* **115**, 337 (2006).
- [32] K. Sumiyoshi, S. Yamada, H. Suzuki, H. Shen, and S. Chiba, *Astrophys. J.* **692**, 922 (2005).
- [33] K. Nakazato, K. Sumiyoshi, and S. Yamada, *Astrophys. J.* **666**, 1140 (2007).
- [34] P. Wang, W. Thomas, and A. G. Williams, *Phys. Rev. C* **75**, 045202 (2007).
- [35] I. Prigogine and R. Defay, *Chemical Thermodynamics* (London: Longmans Green and Co., 1954).
- [36] J. Adams, *et al.*, (STAR Collaboration), *Nucl. Phys. A* **757**, 102 (2005).
- [37] K. Adcox, *et al.* (PHENIX Collaboration), *Nucl. Phys. A* **757**, 184 (2005).
- [38] C. Bernard, *et al.*, *Phys. Rev. D* **71**, 034504 (2005).
- [39] M. Cheng, *et al.*, *Phys. Rev. D* **74**, 054507 (2006).
- [40] Y. Aoki, G. Endrődi, Z. Fodor, S. D. Katz, and K. K. Szabó, *Nature* **443**, 675 (2006a).
- [41] Y. Aoki, Z. Fodor, S. D. Katz, and K. K. Szabó, *Phys. Lett. B* **643**, 46 (2006b).
- [42] S. M. Ransom, J. W. T. Hessels, I. H. Stairs, P. C. C. Freire, F. Camilo, V. M. Kaspi, and D. L. Kaplan, *Science* **307**, 892 (2005).
- [43] F. Özel, *Nature* **441**, 1115 (2006).
- [44] Y. Sekiguchi and M. Shibata, *Phys. Rev. D* **71**, 084013 (2005).
- [45] Y. Sekiguchi and M. Shibata, *Prog. Theor. Phys.* **117**, 1029 (2007).
- [46] C. L. Fryer, S. E. Woosley, and A. Heger, *Astrophys. J.* **550**, 372 (2001).
- [47] K. Nakazato, K. Sumiyoshi, and S. Yamada, *Astrophys. J.* **645**, 519 (2006).
- [48] Y. Suwa, T. Takiwaki, K. Kotake, and K. Sato, *Publ. Astron. Soc. Japan* **59**, 771 (2007).
- [49] Y. T. Liu, S. L. Shapiro, and B. C. Stephens, *Phys. Rev. D* **76**, 084017 (2007).
- [50] K. Nomoto, N. Tominaga, H. Umeda, K. Maeda, T. Ohkubo, J. Deng, and P. A. Mazzali, *ASP Conf. Ser.* **332**, 374 (2005).
- [51] S. Yamada, *Astrophys. J.* **475**, 720 (1997).
- [52] S. Yamada, H.-Th. Janka, and H. Suzuki, *Astron. Astrophys.* **344**, 533 (1999).
- [53] T. A. Thompson, A. Burrows, and P. A. Pinto, *Astrophys. J.* **592**, 434 (2003).